Applied Surface Science Advances 24 (2024) 100660

Contents lists available at ScienceDirect

Applied Surface Science Advances

journal homepage: www.sciencedirect.com/journal/applied-surface-science-advances

Full Length Article

Submicron periodic structures in metal oxide coating via laser ablation and thermal oxidation

Julianija Nikitina [a], Simonas Indrišiūnas [a], Tomas Tolenis [a,c], Mindaugas Andrulevicius [b], Lina Grineviciute [a,*]

[a] Center for Physical Sciences and Technology (FTMC), Savanoriu Ave. 231, LT-02300 Vilnius, Lithuania
[b] Institute of Materials Science, Kaunas University of Technology, K. Barsausko st. 59, LT-51423 Kaunas, Lithuania
[c] ELI Beamlines Facility, Extreme Light Infrastructure ERIC, Za Radnicí 835, 252 41 Dolní Břežany, Czech Republic

ARTICLE INFO

Keywords:
Thin films
Direct laser interference patterning
Submicron linear grating
Thermal oxidation

ABSTRACT

Nano- and micro-structuring of transparent glass for IR or visible spectrum applications is challenging due to low yield and slow processes, especially while maintaining high surface quality. The method proposed in this work involves the structuring and subsequent thermal oxidation of a thin metallic layer on a glass substrate. Annealing of the structured metal layer produces a transparent fully inorganic oxide surface with periodic patterns, avoiding the subtleties of glass structuring. A new method for the formation of sub-micrometer non-absorbing gratings with 750 nm periodicity is presented by direct laser interference patterning (DLIP) of thin tantalum layers on fused silica substrates followed by thermal oxidation by annealing. This method aims to improve the field of laser optics by providing a scalable and efficient method for the creation of precise metal-oxide photonic structures.

1. Introduction

The manipulation of external structure of thin films by periodic structural modifications represents a frontier in science and technology. This technology holds the perspective for fabricating innovative optical elements such as photonic crystals [1–3]. Photonic crystals, characterized by periodic dielectric or metal-dielectric nanostructures, can control light propagation similarly to electron motion, which is controlled by periodic potentials in semiconductor crystals. One-dimensional photonic crystals have found widespread applications in the optical coating industry, particularly in terms of planar multilayer interference coatings, offering applications based on their anti-reflective (AR) or highly reflective (HR) properties [4]. Moreover, the scientific community is exploring two- and three-dimensional photonic crystals [5,6]. Demonstrated advancements include the formation of two-dimensional photonic crystals through physical vapour deposition on pre-patterned substrates [7,8]. Such dielectric structures, featuring periodic modulation of optical constants, exhibit angular selectivity of light, which can be used for spatial filtering [9] and polarization control [10].

The photonic crystal structures, designed for laser optics applications, have to be compatible with strict requirements necessary for high-power lasers. The most crucial criteria for optical elements designed for high-power laser optics applications are to be non-absorbing and durable, which requires the complete inorganic composition of all constituent materials. Elements made from polymers or hybrid-polymer materials are known to exhibit lower resistance to laser fluence compared to fully inorganic elements [11]. Furthermore, variations in resistance to laser radiation among inorganic materials based on their band gap introduce an additional consideration [12]. These requirements are set for both: coating materials and substrates. This means that photonic crystals constituent parts such as optical glasses or various oxides used in optical coatings have to be inorganic and non-absorbing for the target wavelengths.

Direct microstructuring of glass, while keeping the surface roughness sufficiently low is a challenging issue, particularly if the microstructure is needed for the infrared or visible spectrum. However, various oxides used in the optical coatings can be used to make this challenge easier. Instead of microstructuring a glass surface the thin metallic layer deposited on it can be structured. Subsequent annealing of the modulated metal layer promotes metal oxidation, resulting in a fully inorganic, transparent, and periodically modulated surface. A similar approach was shown in the recent work by Okatani et al. [13],

* Corresponding author.
E-mail address: lina.grineviciute@ftmc.lt (L. Grineviciute).

https://doi.org/10.1016/j.apsadv.2024.100660
Received 31 July 2024; Received in revised form 31 October 2024; Accepted 8 November 2024
Available online 20 November 2024

Table 1
Annealing process parameters.

ID	Annealing temperature, °C	Heating rate, °C/min	Annealing duration, h
1	500	2	1
2	600	2	1
3	700	2	1
4	600	3	1
5	600	4	1

demonstrating the fabrication of reflective meta lens for the visible spectrum by thermal oxidation of silicon nanopillars. Such an alternative approach of microstructuring metal layers and annealing helps to avoid the complexities of glass modification, offering a promising avenue for achieving precise periodic patterns. Moreover, periodic structures such as seed layers for 2D photonic crystal formation can be formed on fused silica and other glasses or crystal surfaces.

There are several patterning techniques, described in the scientific literature, that can be used for thin metal film patterning. However, in the fabrication of sub-micrometer size gratings, which are needed for VIS and IR range optical elements, it is difficult to find a technique suitable for high-volume manufacture while providing sufficient quality. UV lithography and subsequent etching through the mask is a well-established method capable of producing sub-micrometer metal patterns, however, the residue of photoresist reduces the damage threshold of the structure. Moreover, nanoimprint technologies are still searching for high laser-induced damage threshold photoresists [14]. Ion beam milling is too slow and expensive for large-scale production. Therefore, ultrashort laser processing, and more accurately direct laser interference patterning (DLIP), was selected for the task, described in this paper.

DLIP technique can enhance the fabrication speed of periodic patterns compared to conventional direct laser writing. Obtaining sub-micrometric gratings in tens of mm^2 area using direct laser writing is challenging due to the need for a high NA objective, precise control of the distance from the objective to the sample, and stability of laser and positioning setup parameters over a long processing time. DLIP allows to avoid these problems. Interference patterning uses the distribution of

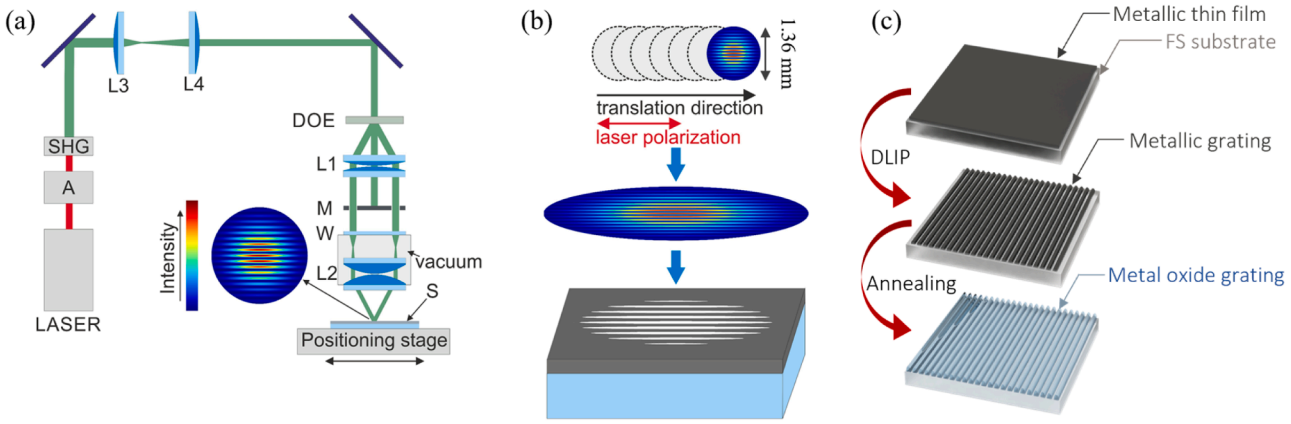

Fig. 1. (a) 2-beam DLIP setup: A – optical attenuator, SHG – generation of second harmonics, L3 and L4 telescope, L1 and L2 objectives of the 4f interference setup, M – beam mask, W – transparent window, S – sample; (b) illustration of grating fabrication in a thin film on a transparent substrate using a 2-beam interference spot scan; (c) manufacturing steps to form metal-oxide submicron gratings from metallic thin film.

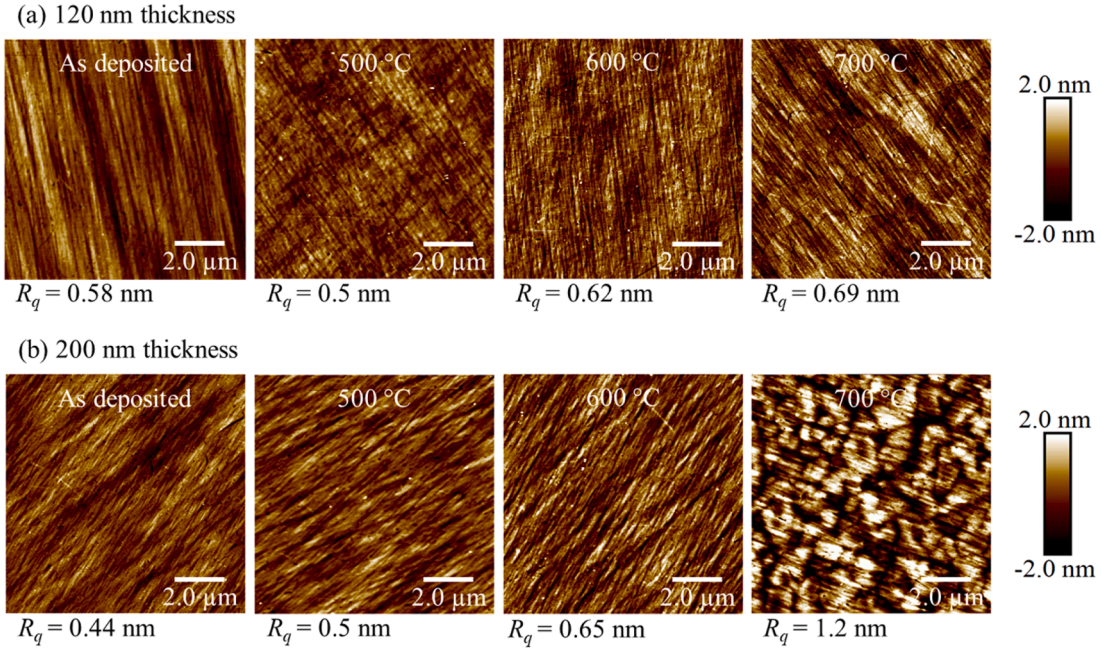

Fig. 2. Typical surface morphologies of (a) 120 nm and (b) 200 nm physical thickness tantalum thin films as deposited and annealed at various temperatures using a 2 °C/min heating rate.

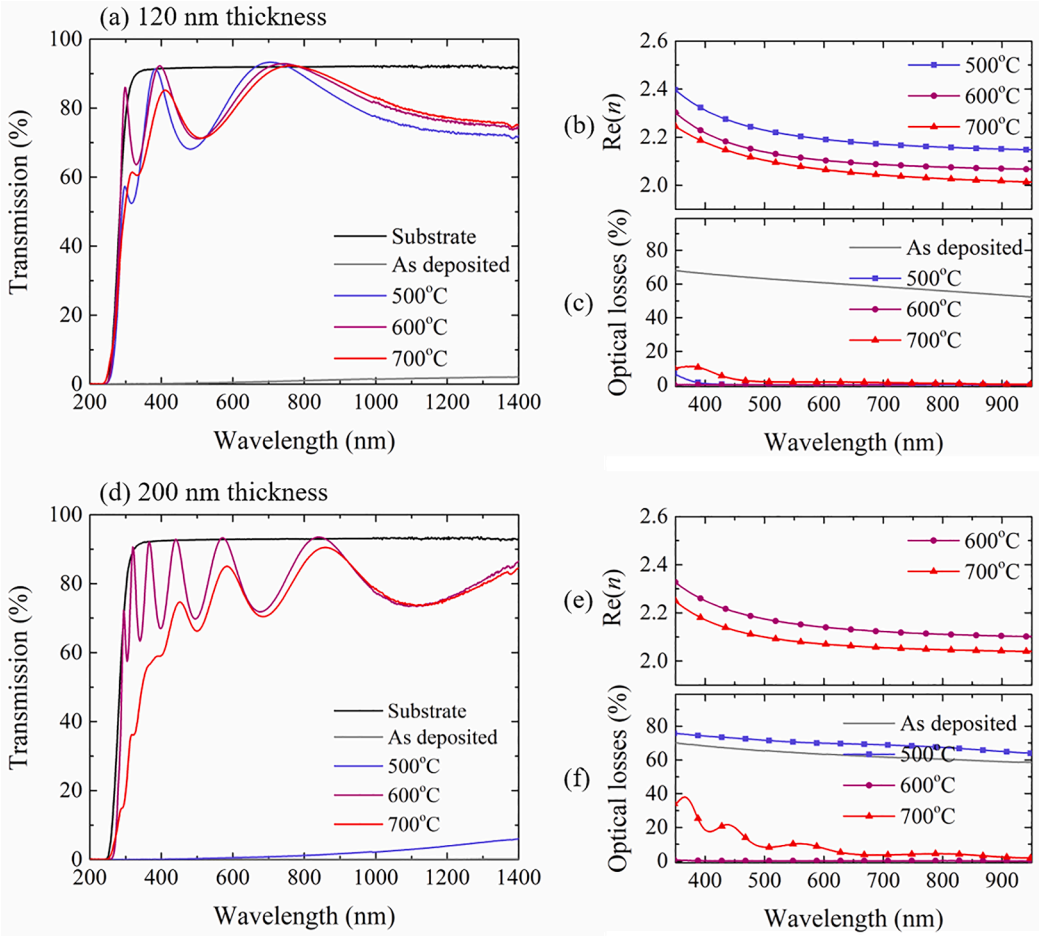

Fig. 3. Transmission spectra of (a) 120 nm (d) 200 nm thick tantalum layers, annealed at various temperatures. Refractive index and optical losses dispersion of (b)-(c) 120 nm (e)-(f) 200 nm thickness tantalum layers, annealed at various temperatures.

Table 2
Structural and optical properties of annealed tantalum thin films.

As grown thickness, nm →	120	200	120	200	120	200
Annealing temperature, °C ↓	Annealed film thickness, nm		Refractive index @ 600 nm		Roughness R_q after annealing, nm	
500	163	–	2.19	–	0.5	0.5
600	177	399	2.10	2.14	0.62	0.65
700	186	418	2.07	2.07	0.69	1.2

irradiation energy over a large fabrication area and produces small features in this area with a single exposition. It also has a much higher focal depth than a laser beam focused using a high NA objective. The spatial period of the interference pattern can be defined by controlling the number of interfering beams, angle between the beams and the laser wavelength. Periods of <200 nm were obtained at 244 nm wavelength [15]. DLIP is widely tested for wetting applications [16], structural color generation [17], fabrication of plasmonic structures [18,19]. DLIP also has potential as a method enabling fast laser microstructuring [20]. To fabricate high-quality submicrometric period linear grating in the bulk material using DLIP is quite a challenging task due to the redeposition of material ejected from the ablation spot, which causes instability of the depth of the grating grooves and corrugations due to heated particles, sticking to the top of the grating. One of the solutions to improve processing quality is to use a thin film deposited on the non-absorbing substrate, which absorbs laser radiation. In this way, the uniform depth of the structure can be much more easily retained by removing material from the top of the substrate. Furthermore, when working with the thin film of high thermal conductivity material deposited on the low thermal conductivity substrate, the film may be heated to the melting temperature. The surface tension of the melted metal depends on its temperature [21] and is higher in the interference minima (cold zones) than in the interference maxima (hot zones). Therefore, molten material flows to the low-temperature sites, corresponding to the minima in the interference pattern due to the Marangoni convection effect [22]. In this way, the grating surface can be more smooth than simply using local material removal.

Therefore, in this work, the technique for forming sub-micrometer metal-oxide gratings using DLIP patterning of metallic tantalum thin film, deposited on fused silica substrate, and subsequent oxidation through thermal annealing was investigated.

2. Materials and methods

2.1. Sample preparation

Tantalum pentoxide is known for its high refractive index and negligible extinction coefficient across a broad spectrum, including visible and infrared regions. This makes it a suitable material for high-performance dielectric metasurface optics in these spectral regions [23]. In this work, we have chosen tantalum material film deposited on UV-Grade Fused Silica (UVFS) substrates for a proof-of-concept. Thin tantalum films of two different physical thicknesses (~120 nm and ~200 nm) were formed on fused silica (UVFS) substrates by ion beam sputtering technology (IBS). To evaluate optimal annealing conditions,

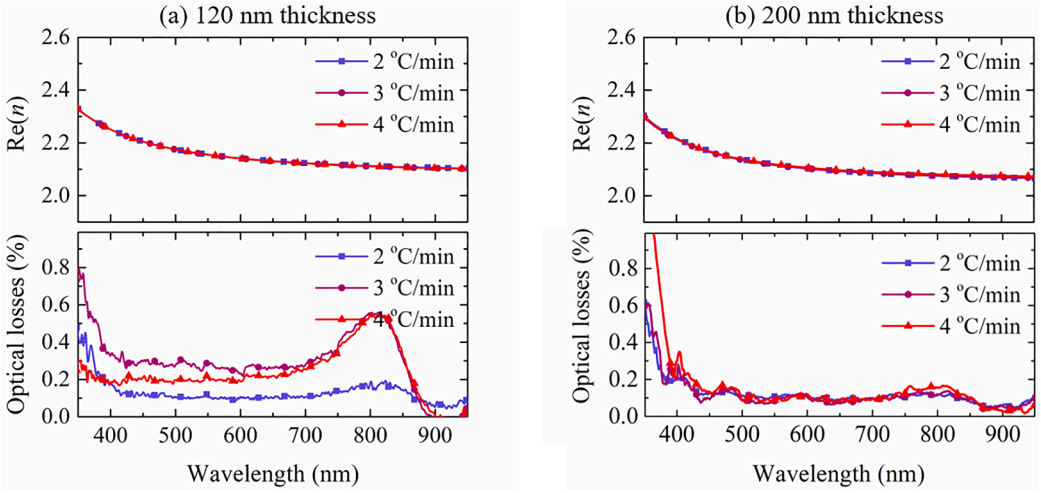

Fig. 4. Refractive index and optical losses dispersions of (a) 120 nm (b) 200 nm thick tantalum layers, annealed using various heating rates.

Table 3
Calculated surface atomic concentrations of tantalum metal thin films before and after annealing.

Sample Nr.	Phys. thickness, nm	Annealing temperature, °C	O, at. %	Ta, at. %
1	200	–	65.54	34.46
2	200	500	72.97	27.03
3	200	600	75.76	24.24
4	200	700	76.11	23.89
Theoretical Ta_2O_5	–	–	71.4	28.6

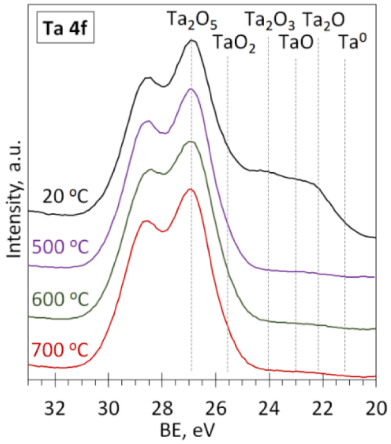

Fig. 5. XPS spectrum of Ta film made by IBS before and after annealing at various temperatures.

which would later be used for structured film samples, the as-grown thin film samples were thermally annealed in an ambient atmosphere in various conditions, summarized in Table 1. The annealing temperature ranged from 500 °C to 700 °C to achieve optically transparent tantalum oxide thin films still in an amorphous phase. Afterwards, samples were slowly cooled in the furnace to the room temperature. Before and after any processing, samples were characterized for structural and optical properties.

2.2. Gratings fabrication by ultrashort pulse laser

For the production of gratings in the tantalum thin film ultrashort pulse laser CYRA DUO (AMPLIGHT KG) was used. The pulse duration of the pulses was set to 7 ps, and the laser was working at a 1000 Hz pulse repetition rate and produced 6 mJ energy pulses. The experiment used an externally generated second harmonic (wavelength 515 nm). A laser beam was split into two using a diffractive optical element (DOE). The first diffractive order beams were collected and overlapped on the sample using a 4f lens setup with a magnification of 4, consisting of two objectives with effective focal lengths of 150 mm (L1) and 37.5 mm (L2). Zero order and not needed high order beams emanating from the DOE, were blocked by a metal mask positioned between the 4f lenses. To avoid plasma generation in air at the focal position of the objective L1, a 200 mbar vacuum was formed between a transparent window W (both sides of which were coated with an anti-reflective coating) and an objective L2 (Fig. 1a). The two beams interfering on the sample formed a line intensity pattern, which was used to produce gratings in the tantalum thin film by translating the sample along the direction of the interference lines, as shown in Fig. 1b. The sample was translated using PLT165 300 DLM-L (Steinmeyer Mechatronik GmbH) translation stage. The translation direction was parallel to the polarization vector of the linearly polarized laser beam. The laser spot size diameter on the sample at $1/e^2$ level was 1.36 mm. The period of the linear interference pattern on the sample was 750 nm. The depth of the produced gratings was varied by changing the pulse energy (irradiation fluence) and translation speed.

After forming the gratings by DLIP, the last step was to anneal the fabricated metallic structure to complete oxidation to form non-absorbing gratings (Fig. 1c). The structured films were annealed using the optimal parameters obtained from the investigation of as-grown films.

2.3. Surface and structure characterization

Atomic force microscopy (AFM). The surface morphology of thin films before and after annealing as well as grating structure were characterized by an atomic force microscope (Dimension Edge, Bruker). The AFM tip Tap300DLC was used, which has a truncated cone shape with a tip radius of <15 nm and a half cone angle at the apex of 10° These measurements were performed in tapping mode in two different 10 μm × 10 μm surface areas.

X-ray photoelectron spectroscopy (XPS). The surface of the thin tantalum films was analyzed before and after thermal treatment using XPS. The KRATOS ANALYTICAL XSAM800 spectrometer with non-monochromatized Al Kα radiation ($h\nu$ = 1486.6 eV) was utilized. The energy scale of the system was calibrated based on the Au $4f_{7/2}$, Cu $2p_{3/2}$, and Ag $3d_{5/2}$ peaks positions. Detailed spectra in the Ta 4f and O 1 s

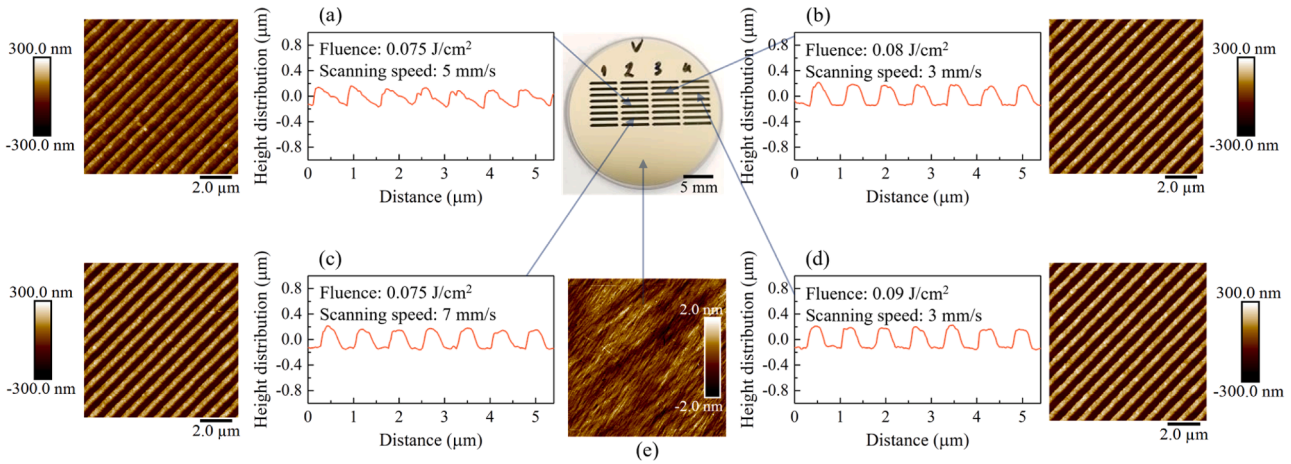

Fig. 6. AFM surface morphology images of the one-inch diameter sample with a series of periodic submicron structures formed by two-beam interference ablation of 200 nm thickness tantalum film. The insets indicated by the arrows (a)-(d) show 2D surface morphologies and 1D surface profiles of the periodic structures formed with the corresponding DLIP power and scanning speed parameters; (e) planar surface of the film.

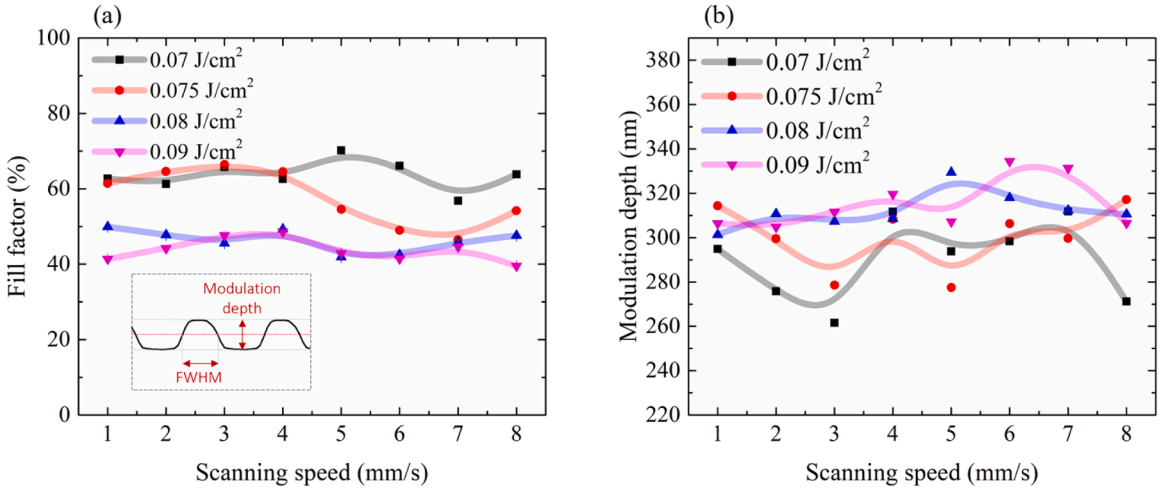

Fig. 7. (a) Fill factor and (b) modulation depth of ablated gratings dependencies on pattering parameters (fluence and scanning speed).

regions were obtained using a 20 eV pass energy with a 0.1 eV energy increment, and the analyzer was set to the fixed analyzer transmission (FAT) mode.

Spectrophotometric measurements. Optical transmittance and reflectance were evaluated within the 200 – 1200 nm spectral range for an unpolarized light at an 8° incidence angle using a Photon RT spectrophotometer (Essent Optics, Lithuania).

3. Results and discussion

3.1. Planar thin film annealing

The initial investigation aimed to estimate the optimal annealing temperature for oxidation of as-grown tantalum thin films avoiding formation of polycrystalline structure. Fig. 2 shows AFM surface roughness images of non-annealed and annealed at 500 °C, 600 °C and 700 °C temperatures samples. Samples annealed at 500 °C and 600 °C had surface morphology similar to the as-grown samples, with insignificant surface roughness changes. After treatment at 700 °C for 1 h, surface morphologies indicated structural changes such as cracks/defects formation, significantly increased surface roughness for 200 nm-thick film. Structural alterations at 700 °C annealing temperature must be caused by the amorphous material reorganization into (poly) crystalline structure, showing contouring grains boundaries, which correlate with the results demonstrated in [24–26].

Correspondingly, as shown in spectrophotometric measurements in Fig. 3(a, d), transmission spectra of thin films annealed at 700 °C have decreased in transmission, which can be attributed to increased light scattering from the rough surface and the polycrystallinity of Ta_2O_5. The refractive index of film oxidized at 700 °C ($n \approx 2.07$) is lower compared to the film oxidized at 600 °C ($n \approx 2.14$) at 600 nm wavelength (Fig. 3b). This tendency has been observed in similar material science papers: annealing at temperatures above 650 °C can initiate a polycrystalline state of the material, with a lower refractive index due to the reduced density [25,27] (Table 2).

Both 200 nm-thick and 120 nm-thick samples annealed at 600 °C and 120 nm-thick sample annealed at 500 °C showed high transparency with minimal optical losses (Fig. 3(a-f)). On the other hand, as-grown 200 nm thick tantalum thin film annealed at 500 °C still had substantial optical losses in the whole spectrum as shown in Fig. 3(d, f) and remained visually "metallic" to the naked eye. 600 °C temperature for thermal oxidation showed the most promising results since samples of both thicknesses were optically transparent with minimal optical losses.

The earlier used heating rate of 2 °C per minute is a safe value for most optical samples, although only the ramp-up stage up to 600 °C takes almost 5 h. To optimize the treatment procedure, faster heating

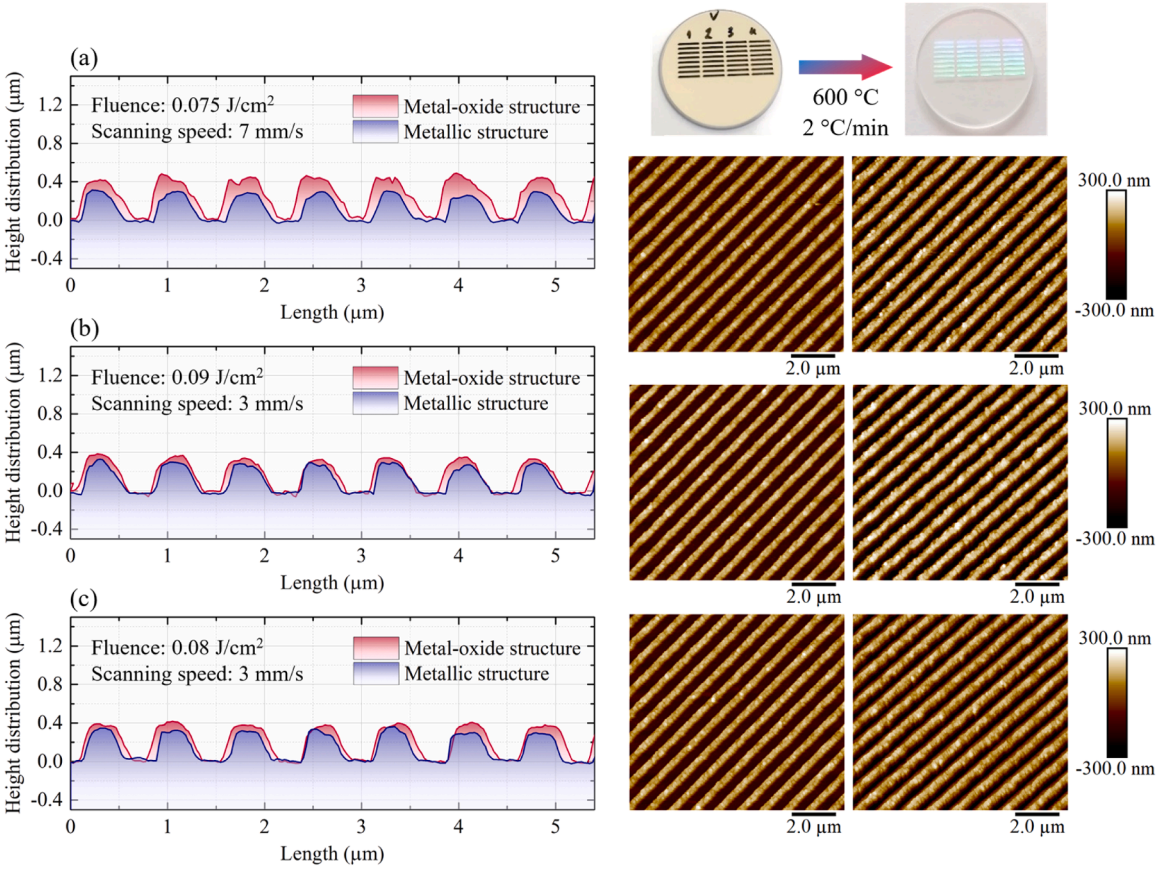

Fig. 8. The comparison of 2D surface patterns before and after thermal oxidation.

rates (3 °C/min and 4 °C/min) were tested. Fig. 4 shows the comparison of optical characteristics of the samples annealed at 600 °C with various heating rates. As can be seen, refractive index values do not change with the heating rate for both sample thicknesses. However, the optical losses tended to slightly increase, when higher heating rates were used. For both film thicknesses the optical losses increased in the 400 – 900 nm spectral range when using 3 and 4 °C/min rates, compared to the 2 °C/min rate.

3.2. Planar thin films' chemical composition before and after annealing

XPS measurements were carried out to investigate the observed decrease in optical losses and to evaluate the absence of suboxides or metallic inclusions at optimum annealing temperatures. Tantalum thin films were characterized by XPS before annealing and after annealing at 500 °C, 600 °C, and 700 °C under ambient conditions using 2 °C/min annealing rate. Surface atomic concentrations for different samples are shown in Table 3.

The surface atomic concentrations for all samples appeared to be similar to those of stochiometric tantalum pentoxide, except for the sample before annealing. This could be explained by the fact that the deposited tantalum metal film oxidizes in the ambient atmosphere, forming a natural oxide film (approximately one or two nanometers) before any annealing procedure. This means that before annealing, the deposited Ta film has a higher metal content and is not stoichiometric (Table 3). During the annealing procedure, the oxygen diffuses into the depth of the metal film, thus forming a thicker oxide layer. This results in an increased amount of oxygen on the surface of the film for all annealed samples (Table 3).

For a more detailed analysis of the Ta oxidation state, the detailed XPS spectra in the Ta 4f region were scanned and compared for 200 nm thick films before and after the annealing procedure (Fig. 5). The positions of the Ta 4f7/2 peaks for different tantalum oxidation states, indicated in this picture, are explained in detail by Li et al. [28]. The comparison results showed a decrease in the concentration of tantalum suboxides after the annealing processes. This decrease of suboxides (Ta_2O, TaO, Ta_2O_3) is correlated with increased transmittance (decreased optical losses). This finding aligns with prior research, indicating that suboxides tend to absorb visible light and pure stoichiometric Ta_2O_5 is transparent for the wavelength range 400–2500 nm [29].

Investigation of the structural, optical, and chemical characteristics of various annealing procedures applied to tantalum thin films offered insights into the optimal parameters for thin film thermal oxidation. To avoid high optical losses and reach the purest Ta_2O_5 composition, 600 °C annealing temperature and 2 °C/min heating rate were used in thin film structuring experiments.

3.3. Structured thin film annealing

According to the procedure, described in Section 2.2, tantalum thin films were patterned by DLIP. Figs. 6–8 summarize the morphological characteristics of submicrometer linear gratings formed in 200 nm-thick tantalum film. Four different fluence values and 8 different scanning speed values were used in these experiments.

Periodic gratings with surface modulation on a wavelength scale: spatial period ~750 nm, fill factor ~50 %, and 260 – 300 nm modulation depth were fabricated. The filling factor was calculated at half maxima of modulation depth (red dotted line in a sketch in Fig. 7a). The variation of grating characteristics and their dependency on fabrication parameters (fluence and scanning speed) are shown in Fig. 7 The modulation depth surpassed the initial film thickness (200 nm) in all cases. This shows that the melting of Ta film was an important factor in

the grating formation. The fill factor was practically independent of the scanning speed and tended to reduce from 60 % to 40 % when fluence increased from 1.1 to 1.4 J/cm^2. The molten metal was more efficiently pushed to the low-intensity areas when fluence was high. This is also confirmed by the increased modulation depth when using high fluence.

The patterned tantalum thin film sample was annealed using earlier estimated parameters: 2 °C per minute heating rate up to 600 °C, held for an hour, and cooled down to room temperature along with the furnace pace. Afterwards, captured surface morphologies of structured areas showed increased modulation depths and fill factor (Fig. 8). As it is inevitable during the oxidation process, attachment of oxygen atoms to metal causes material volumetric expansion. Generally, the modulation depth average has increased from 280 nm up to 420 nm, and the fill factor has increased by approximately 10 % (from 50 % to 60 %).

This method could be expanded for fabrication of different periodicity or even 2D structures, such as metasurfaces, at least to IR spectral band. Slightly smaller periodicities can be relatively easily achieved and much smaller (i.e. by factor of 10) periodicities cannot currently be easily fabricated using this method. DLIP can provide 2D patterns [30], therefore, this method can be used for 2D non-absorbing gratings. However, if large area (square centimeter or more) is needed, 1D grating pattern is less technologically challenging, since the interference spot can be simply translated in the direction parallel to the grooves to pattern long area (Fig. 1b), so the stitching of the pattern is required only in one direction. Furthermore, DLIP does not provide much flexibility in pattern shape, although the flexibility can be somewhat increased using phase or polarization control for each of the beams [31,32]. Another possibility to produce required pattern shape is to reposition the sample between the laser expositions. This can be done by rotating the sample or by moving the sample in steps, smaller than the pattern period [33, 34]. One more issue would be ensuring the variable fill factor, which is often needed in metasurfaces. To achieve this, some kind of beam shaping or manipulation of the Gaussian beam would be needed.

4. Conclusions

The new method for nano-structuring films on glass substrates has been successfully demonstrated. It allows to efficiently fabricate fully inorganic periodic photonic structures on larger scale. Direct laser interference patterning of metal layer followed by thermal oxidation by annealing has been proven to be an effective method for obtaining the sub-micrometer (750 nm period) non-absorbing gratings. No absorption has been detected by spectrophotometric measurements, which allows to use the developed nanostructures for high intensity laser optics applications. The findings show that this method can overcome the problems associated with traditional glass microstructuring and is a promising route for the development of advanced optical elements. Future work should focus on improving the DLIP process to increase the uniformity in large areas and quality of the grating, as well as investigating its applicability to other materials such as silicon, hafnium, etc.

CRediT authorship contribution statement

Julianija Nikitina: Writing – review & editing, Methodology, Data curation. **Simonas Indrišiūnas:** Writing – review & editing, Methodology. **Tomas Tolenis:** Writing – review & editing, Methodology. **Mindaugas Andrulevicius:** Writing – review & editing, Data curation. **Lina Grineviciute:** Writing – review & editing, Writing – original draft, Supervision, Investigation.

Declaration of competing interest

The authors declare that they have no known competing financial interests or personal relationships that could have appeared to influence the work reported in this paper.

Acknowledgements

This work was supported by the PerFIN project from the Research Council of Lithuania (LMTLT), agreement No S-MIP-22–80.

Data availability

Data will be made available on request.

References

[1] M. Kim, Z. Jacob, J. Rho, Recent advances in 2D, 3D and higher-order topological photonics, Light Sci. Appl. 9 (130) (2020) 2047–7538, https://doi.org/10.1038/s41377-020-0331-y.
[2] G.J. Tang, X.T. He, F.L. Shi, J.W. Liu, X.D. Chen, J.W. Dong, Topological photonic crystals: physics, designs, and applications, Laser Photon. Rev. 16 (4) (2022) 2100300, https://doi.org/10.1002/LPOR.202100300. Apr.
[3] M.A. Butt, S.N. Khonina, N.L. Kazanskiy, Recent advances in photonic crystal optical devices: a review, Opt. Laser Technol. 142 (Oct. 2021) 107265, https://doi.org/10.1016/J.OPTLASTEC.2021.107265.
[4] N. Kaiser, H.K. Pulker, Optical Interference Coatings, 1st ed., Springer, 2014.
[5] J. Li, J. Yan, L. Jiang, J. Yu, H. Guo, L. Qu, Nanoscale multi-beam lithography of photonic crystals with ultrafast laser, Light Sci. Appl. 12 (1) (2023) 1–12, https://doi.org/10.1038/s41377-023-01178-3.
[6] S. Dhuey, et al., Three-dimensional woodpile photonic crystals for visible light applications, J. Phys. Commun. 1 (1) (Aug. 2017) 015004, https://doi.org/10.1088/2399-6528/AA7EF9.
[7] L. Grinevičiūtė, et al., Nanostructured multilayer coatings for spatial filtering, Adv. Opt. Mater. (2021), https://doi.org/10.1002/adom.202001730.
[8] L. Grinevičiūtė, 'Nanostructured optical coatings for the manipulation of laser radiation', dissertation, Vilnius University, Center for Physical Sciences and Technology, 2021.
[9] L. Grinevičiūtė, J. Nikitina, C. Babayigit, K. Staliūnas, Fano-like resonances in nanostructured thin films for spatial filtering, Appl. Phys. Lett. 118 (13) (2021), https://doi.org/10.1063/5.0044032.
[10] D.S. Hobbs, B.D. Macleod, A.D. Manni, and S.M. Consoles, 'Pulsed laser damage resistance of nano-structured polarizers for 1064 nm', 2018, doi: 10.1117/12.2500339.
[11] A. Žukauskas, G. Batavičiute, M. Ščiuka, Z. Balevičius, A. Melninkaitis, M. Malinauskas, Effect of the photoinitiator presence and exposure conditions on laser-induced damage threshold of ORMOSIL (SZ2080), Opt. Mater. (Amst). 39 (2015) 224–231, https://doi.org/10.1016/J.OPTMAT.2014.11.031.
[12] B. Mangote, et al., Femtosecond laser damage resistance of oxide and mixture oxide optical coatings, Opt. Lett. 37 (9) (2012) 1478, https://doi.org/10.1364/ol.37.001478.
[13] T. Okatani, Y. Naito, Y. Kanamori, Fabrication of high-aspect-ratio SiO2 nanopillars by Si thermal oxidation for metalenses in the visible region, Jpn. J. Appl. Phys. 62 (SG) (2023) SG1034, https://doi.org/10.35848/1347-4065/acbfbe.
[14] E. Kabouraki, et al., High laser induced damage threshold photoresists for nano-imprint and 3D multi-photon lithography, Nanophotonics 10 (14) (2021) 3759–3768, https://doi.org/10.1515/nanoph-2021-0263. Oct.
[15] J. de Boor, N. Geyer, U. Gösele, V. Schmidt, Three-beam interference lithography: upgrading a Lloyd's interferometer for single-exposure hexagonal patterning, Opt. Lett. 34 (12) (2009) 1783, https://doi.org/10.1364/OL.34.001783. Jun.
[16] S. Milles, M. Soldera, T. Kuntze, A.F. Lasagni, Characterization of self-cleaning properties on superhydrophobic aluminum surfaces fabricated by direct laser writing and direct laser interference patterning, Appl. Surf. Sci. 525 (2020) 146518, https://doi.org/10.1016/J.APSUSC.2020.146518. Sep.
[17] B. Voisiat, W. Wang, M. Holzhey, A.F. Lasagni, Improving the homogeneity of diffraction based colours by fabricating periodic patterns with gradient spatial period using Direct Laser Interference Patterning, Sci. Reports 2019 91 9 (1) (2019) 1–9, https://doi.org/10.1038/s41598-019-44212-4. May.
[18] Y.-R. Wang, et al., Direct patterning of periodic semiconductor nanostructures using single-pulse nanosecond laser interference, Opt. Express 28 (22) (2020) 32529–32539, https://doi.org/10.1364/OE.397709. *Vol. 28, Issue 22, pp. 32529-32539*Oct.
[19] J. Berzinš, et al., Direct and high-throughput fabrication of mie-resonant metasurfaces via single-pulse laser interference, ACS Nano 14 (5) (2020) 6138–6149, https://doi.org/10.1021/acsnano.0c01993. May.
[20] A.F. Lasagni, Laser interference patterning methods: possibilities for high-throughput fabrication of periodic surface patterns, Adv. Opt. Technol. 6 (3–4) (2017) 265–275, https://doi.org/10.1515/aot-2017-0016.
[21] H.M. Lu, Q. Jiang, Surface tension and its temperature coefficient for liquid metals, J. Phys. Chem. B 109 (32) (2005) 15463–15468, https://doi.org/10.1021/JP0516341. Aug.
[22] C.N. Baroud, Marangoni Convection, Encycl. Microfluid. Nanofluidics (2013) 1–8, https://doi.org/10.1007/978-3-642-27758-0_852-4.
[23] C. Zhang, L. Chen, Z. Lin, et al., Tantalum pentoxide: a new material platform for high-performance dielectric metasurface optics in the ultraviolet and visible region, Light Sci. Appl. 13 (2024) 23, https://doi.org/10.1038/s41377-023-01330-z.

[24] R. Chandrasekharan, I. Park, R.I. Masel, M.A. Shannon, Thermal oxidation of tantalum films at various oxidation states from 300 to 700 °C, J. Appl. Phys. 98 (11) (2005), https://doi.org/10.1063/1.2139834.
[25] E. Çetinörgö-Goldenberg, J.E. Klemberg-Sapieha, L. Martinu, Effect of postdeposition annealing on the structure, composition, and the mechanical and pptical characteristics of niobium and tantalum oxide films, Appl. Opt. 51 (27) (2012) 6498–6507, https://doi.org/10.1364/AO.51.006498.
[26] E. Atanassova, et al., High temperature-induced crystallization in tantalum pentoxide layers and its influence on the electrical properties, Thin. Solid. Films 426 (1–2) (2003) 191–199, https://doi.org/10.1016/S0040-6090(03)00027-0.
[27] J.P. Masse, H. Szymanowski, O. Zabeida, A. Amassian, J.E. Klemberg-Sapieha, L. Martinu, Stability and effect of annealing on the optical properties of plasma-deposited Ta2O5 and Nb2O5 films, Thin. Solid. Films 515 (4) (2006) 1674–1682, https://doi.org/10.1016/j.tsf.2006.05.047.
[28] Y. Li, et al., Tuning the stoichiometry and electrical properties of tantalum oxide thin films, Appl. Surf. Sci. 470 (2019) 1071–1074, https://doi.org/10.1016/J.APSUSC.2018.11.153. Mar.
[29] J.R. Sites, K. Geib, H. Demiryont, Effects of oxygen content on the optical properties of tantalum oxide films deposited by ion-beam sputtering, Appl. Opt. 24 (4) (1985) 490–495, https://doi.org/10.1364/AO.24.000490. *Vol. 24, Issue 4, pp. 490-495*Feb.
[30] B. Voisiat, M. Gedvilas, S. Indrišiunas, G. Raciukaitis, Flexible microstructuring of thin films using multi-beam interference: ablation with ultrashort lasers, J. Laser Micro Nanoeng. 6 (3) (2011) 185–190, https://doi.org/10.2961/JLMN.2011.03.0002. Dec.
[31] S. Indrišiūnas, B. Voisiat, M. Gedvilas, G. Račiukaitis, New opportunities for custom-shape patterning using polarization control in confocal laser beam interference setup, J. Laser Appl. 29 (1) (2017), https://doi.org/10.2351/1.4976679.
[32] Y. Nakata, Interference laser processing, Adv. Opt. Technol. 5 (1) (2016) 29–38, https://doi.org/10.1515/aot-2015-0060.
[33] S. Indrišiunas, B. Voisiat, M. Gedvilas, G. Račiukaitis, Two complementary ways of thin-metal-film patterning using laser beam interference and direct ablation, J. Micromechanics Microengineering 23 (9) (2013) 095034, https://doi.org/10.1088/0960-1317/23/9/095034. Aug.
[34] A. Peter, A.H.A. Lutey, S. Faas, L. Romoli, V. Onuseit, T. Graf, Direct laser interference patterning of stainless steel by ultrashort pulses for antibacterial surfaces, Opt. Laser Technol. 123 (2020) 105954, https://doi.org/10.1016/J.OPTLASTEC.2019.105954. Mar.